Nominal PbSe nano-islands on PbTe: grown by MBE, analyzed by AFM and TEM

Peter Moeck[1], Mukes Kapilashrami[1*], Arvind Rao[1*], Kirill Aldushin[2], Jeahuck Lee[3], James E. Morris[3], Nigel D. Browning[4], and Patrick J. McCann[5]

[1] *Portland State University (PSU), Department of Physics, P.O. Box 751, Portland, OR 97207-0751, USA (pmoeck@pdx.edu), * Department of Materials Science, The Royal Institute of Technology, Brinellvägen 23, S-100 44 Stockholm, Sweden*
[2] *Institut für Geologie, Mineralogie und Geophysik der Universität Bochum, Universitätsstraße 150, D- 44780 Bochum, Federal Republic of Germany*
[3] *Portland State University, Department of Electrical & Computer Engineering, P.O. Box 751, Portland, OR 97207-0751, USA*
[4] *Department of Chemical Engineering and Materials Science, University of California at Davis, One Shields Avenue, Davis, CA 95616; and National Center for Electron Microscopy, MS 72-150, Lawrence Berkeley National Laboratory, Berkeley, CA 94720, USA*
[5] *University of Oklahoma, School of Electrical and Computer Engineering, Norman, OK 73019, USA*

ABSTRACT

Nominal PbSe nano-islands were grown in the Stranski-Krastanow mode on (111) oriented PbTe/BaF_2 pseudo-substrates by molecular beam epitaxy (MBE). The number density and morphology of these islands were assessed by means of atomic force microscopy (AFM). Transmission electron microscopy (TEM) was employed to determine the strain state and crystallographic structure of these islands. On the basis of both AFM and TEM analyses, we distinguish between different groups of tensibly strained islands. The suggestion is made to use such nano-islands as part of nanometrology standards for scanning probe microscopy.

INTRODUCTION

Heteroepitaxial semiconductor quantum dots have over the last decade resulted in "*paradigm changes in semiconductor physics and technology*" [1]. Improved optoelectronic devices (such as lasers and mid-infrared detectors) and novel nanoelectronics concepts which depend on single electron transport and tunneling have been demonstrated [1-5]. The PbSe/PbTe quantum dot system [6-9] is particularly interesting for mid-infrared vertical cavity surface emitting lasers [10]. Unlike most III-V and II-VI compound semiconductor quantum dot systems, strong confinement of both holes and electrons can readily be achieved in lead salt quantum dots. The Bohr radii of the holes and electrons are of the same order of magnitude, resulting for PbSe in an exciton Bohr radius on the order of 50 nm.

Materials science aspects of heteroepitaxial quantum dot growth are extensively discussed in the above mentioned reviews [1-5], but atomic ordering and phase separation in such heteroepitaxial structures are a rather new field of study [11-13]. This is surprising, as it has been known since 1985 that atomic ordering and phase separation exists in basically all technically important heteroepitaxial column IV element, III-V, and II-VI compound semiconductor alloy structures that possess in the disordered state the diamond or sphalerite (zinc blende) structure [14,15]. Atomic ordering [16] and phase separation [17] in IV-VI compounds with the halite (rock salt) structure has, to our knowledge, only been reported twice in epitaxial (Pb,Eu)Te. Note that while typical heteroepitaxial growth of quantum dots proceeds in the Stranski-Krastanow growth mode under compressive stress, there is a tensile stress on nominal PbSe islands and wetting layers on a PbTe/BaF_2 pseudo-substrate. This results in a tensile strain of a few percent for nominal PbSe quantum dots. As in the better studied (compressively strained) III-V quantum dot systems, e.g. [18], there is most likely also alloying in both the wetting layer and the islands. This alloying will tend to reduce the nominal stresses and strains.

For simplicity, we will consider both the 3D islands and the 2D wetting layer as being composed of Pb(Se,Te). When such islands are overgrown with a semiconductor material with larger band gap and lattice constant such as PbTe, tensibly strained quantum dots are obtained. We will, therefore, refer to the Pb(Se,Te) islands on a Pb(Se,Te) wetting layer of this study below as predecessor structures of quantum dots. In this paper we report results of AFM studies of such a sample. TEM results from both the nano-island and the wetting layer of the same sample will also be presented.

EXPERIMENTAL DETAILS

The nominal PbSe islands on PbTe were grown by means of MBE at the University of Oklahoma using PbTe, PbSe and Se sources. Freshly cleaved (111) oriented BaF_2 was used as the substrate. After desorption of surface layers for 15 minutes at 500 °C, a 2.67 μm thick, lattice matched $PbTe_{0.22}Se_{0.78}$ buffer layer was grown at 400 °C

and a growth rate of 0.278 nm s^{-1}. At the same temperature, 1.8 μm Se doped PbTe was grown at a rate of 0.167 nm s^{-1}. Then the temperature was lowered to 380 °C and 0.8 nm (2.6 ML) PbSe was deposited at a rate of 0.027 nm s^{-1}. The sample was finally cooled down to room temperature at a rate of 1 K s^{-1}.

AFM studies were performed both at Portland State University and the University of Bochum (Germany) using the non-contact, tapping, and contact modes of a Quesant Q-Scope™ 250 and a Digital Instrument Nanoscope II. A so called "PointProbe® Plus" tip (with a nominal radius of < 10 nm, full tip cone angle at the apex of 20°) was used as the scanning probe in the Digital Instruments AFM. A variety of different types of scanning Si tips were employed in the Quesant AFM in order to assess convolution effects, which are as such unavoidable [19], between the shape of the AFM tips and the shape of the islands. In total, a sample area of approximately 150 μm^2 was assessed with both AFMs. Ten different areas to one μm^2 each were selected for representative island dimension measurements with the Quesant AFM.

From the Pb(Se,Te) quantum dot predecessor structure, [111] plan-view TEM specimens were prepared by standard mechanical grinding and ion-milling techniques. These specimens were analyzed in a JEOL JEM-3010 TEM at 300 kV at the Research Resources Center of the University of Illinois at Chicago (UIC).

RESULTS AND DISCUSSIONS

AFM assessments

Figs. 1a,b were recorded with the Quesant AFM employing a so called "NSC15 tip" (with a nominal radius of < 10 nm, full tip cone angle at the apex of 30°). Figs. 2a,b, on the other hand, were obtained with the Digital Instruments AFM and show two distinctly different surface topographies. The sample surface topography in Fig. 2a compares well with that shown in Figs. 1a,b, and represents the majority of assessed sample areas. Smaller and lager islands with apexes coexist, Fig. 1b, and occasionally there are a few very tall islands with apexes, Fig. 2a. In addition to small islands with apexes, Fig. 2b shows several large flat-toped islands, which could well be the results of the coalescence of islands with apexes. The insets in Figs. 2a,b are corresponding plots of island height versus base widths diameter as obtained from the Quesant AFM from areas of one μm^2. As there was just one area with such large flat-topped islands (1 μm^2), inset to Fig. 2b, amongst the 10 investigated one μm^2 areas, it is fair to conclude that this is the minority surface topography.

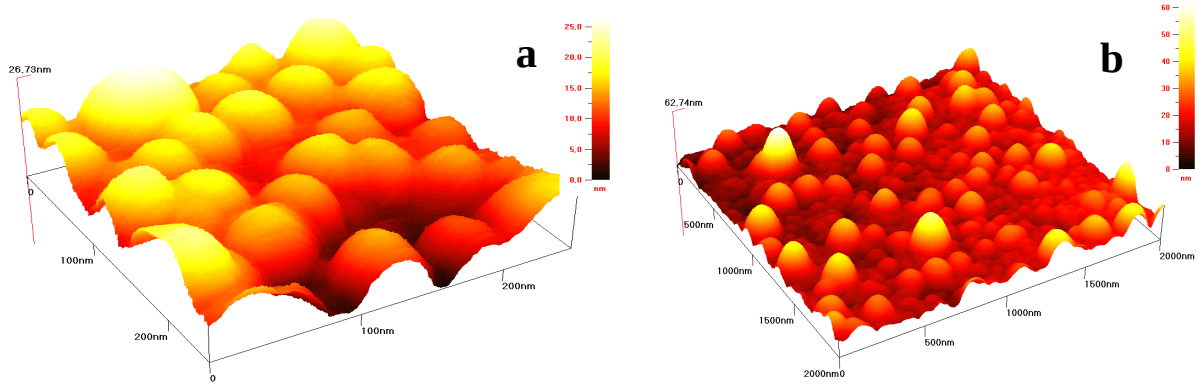

Figure 1. Tapping-mode AFM images of sections of the Pb(Se,Te) quantum dot predecessor structure as obtained from the Quesant AFM. Note the increasing height scale in these images with increased imaged area from **(a)** maximal 26.73 nm over 0.06 μm^2 to **(b)** maximal 62.74 nm over 4 μm^2.

On the basis of the AFM measurements, we classify the islands into three groups according to peaks in the height histograms of the islands that were present in the selected 10 one μm^2 sample areas. For simplicity we refer to these groups as: small, medium-height, and tall islands. Small islands possess a number density of 14.6 μm^{-2} and have an average height (h) of 8.2 nm with a standard deviation (σ) of 1.6 nm, resulting in a relative spread (σ/h) of 19.5 %. Medium-height islands are with a number density of 126.9 μm^{-2} in the majority and possess an average height of 16.9 nm with a standard deviation of 4.6 nm and a relative spread of 27.2 %. Tall islands possess a number density of 16.8 μm^{-2} and have an average height of 41.1 nm, standard deviation of 10.9 nm, and relative spread of 26.5 %. While the combined histogram of all 1583 measured islands is shown in Fig. 3a, Fig. 3b gives a plot of these island heights versus base widths diameters. Note that the average height of the medium-height islands compares well to the average height of the flat-topped islands, Fig. 2b and its inset, as one would expect it to be if the flat-topped islands resulted from the coalescence of islands with apexes. Trigonal pits in flat-topped islands, arrow in Fig. 2b, are another indication that island coalescence may have taken place.

Mainly the tall islands, e.g. such as the one that is marked by an arrow in Fig. 2a, revealed {100} facets as earlier observed on similar samples by other authors [6,7]. This indicates that there are significant convolution effects for most medium-height and small islands. The high number density of the islands is here to be taken into

account as well. Cleary, for tall and therefore "partly free standing" islands not only do the dimensions of the AFM tip become smaller than those of these islands, but also there are hardly any tall neighboring islands around that may influence the scanning tip. Due to the trigonal-pyramidal geometry of epitaxial {100} faceted islands on (111) oriented substrates [6,7], height-to-widths aspect ratios of 0.471 (marked in Fig. 3b) are to be expected.

For our assessment of scanning AFM tip – island shape convolution effects, we employed so called "sting tips" of nominal radii of < 4 nm, extra sharp tip heights of > 600 nm, and so called "high resolution tips" of nominal radii of 1 nm and extra sharp tip heights of 100 to 200 nm. As expected, sharper tips resulted for typical sample areas in larger island height-to-widths aspect ratios. When compared to the island height-to-widths aspect ratios that were obtained with the NSC15 tips, these aspect ratios were on average approximately 40 % higher for scans with the sting tip and twice as high for scans with the high resolution tips.

We expect that optimization of the MBE growth procedure shall result in island distributions as uniform as reported by other authors [6-9]. Since the imaging of nanometer sized {100} faceted island with apexes was challenging, such a sample could serve as an AFM nanometrology standard. Certain crystallographic directions would have to be marked for this purpose on such a sample by some means such as, e.g., partial cleavage [20].

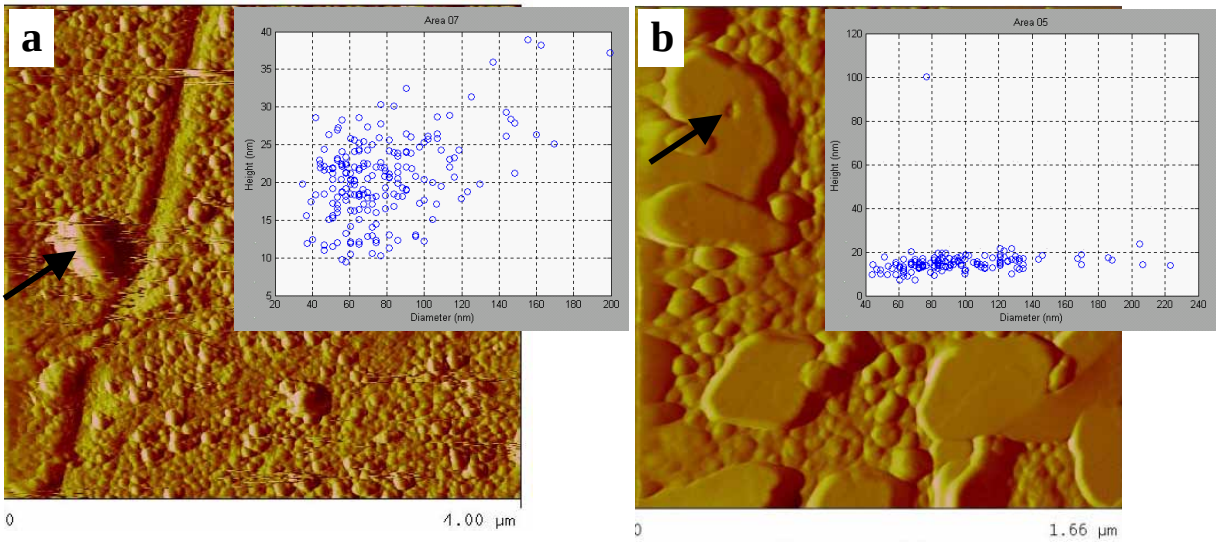

Figure 2. Contact-mode AFM images of approximately 16 µm^2 **(a)** and 2.75 µm^2 **(b)** wide sections of the Pb(Se,Te) quantum dot predecessor structure as obtained from the Digital Instruments AFM. While area **(a)** represents the majority surface topography with islands with distinct apexes, area **(b)** shows the minority surface topography were the large islands are all flat-topped. The arrows mark a trigonal-pyramidal island in **(a)** and a trigonal pit in **(b)**. The insets are corresponding plots of island height versus base widths diameters as obtained from the Quesant AFM from areas of one µm^2. Comparable results were, thus, obtained with both AFMs.

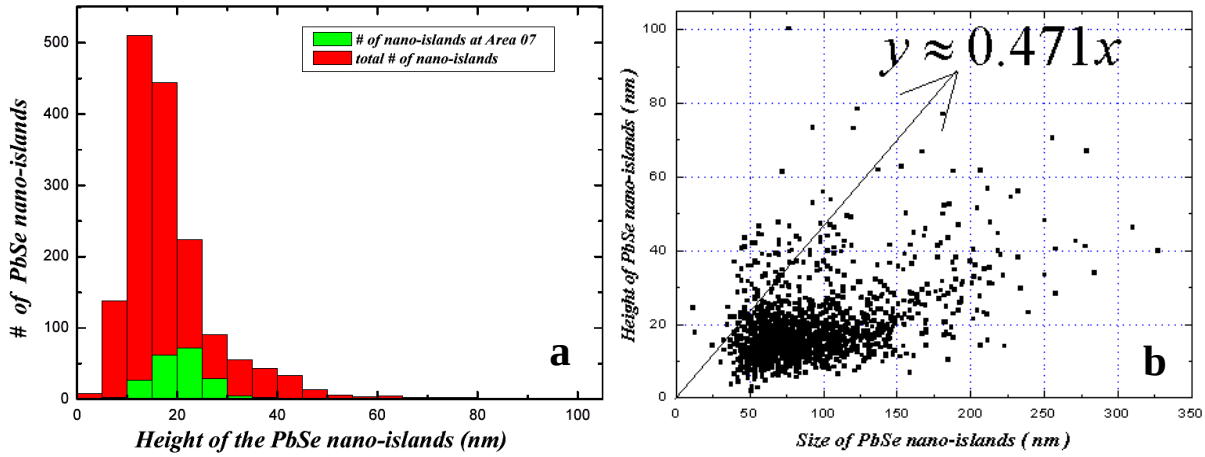

Figure 3. Statistical island parameter overview as obtained with the Quesant AFM and NSC15 tips for the 10 one µm^2 areas. **(a)** Island height histogram showing that most islands are in a height range between 10 to 20 nm. The inset histogram is from the same one µm^2 sample area as that from which the data in the inset of Fig. 2a originate. **(b)** Plot of island height versus base widths diameter. The function $y \approx 0.471\,x$ represents the height-to-widths aspect ratios that one would expect for trigonal-pyramidal islands with {100} facets on a (111) substrate.

TEM study

Fig. 4 shows smaller (revealed by so-called "coffee-bean contrasts") and larger (revealed by so-called "black-white" contrasts) Pb(Se,Te) islands. According to the well known Ashby-Brown theory of strained precipitates, the differences in contrast are due to differences in size. The presence of strained island that can be classified into two different size groups is, thus, confirmed by TEM. As the contrasts in this image show, these two kinds of islands are obviously strained and we call them ordinarily strained islands. They may, thus, be considered to constitute predecessors of ordinarily strained quantum dots. The largest islands that were observed by means of AFM are probably relaxed and may, therefore, not act as quantum dots when overgrown with a larger band-gap semiconductor layer.

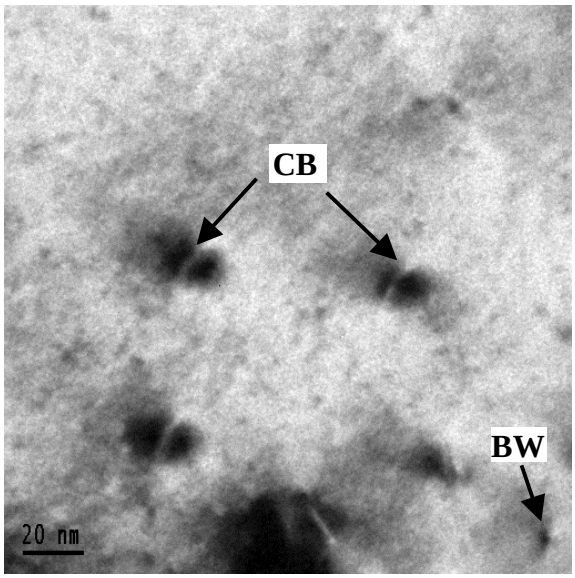

Figure 4. Near [111], {220} dark-field diffraction contrast image of smaller and larger ordinarily strained Pb(Se,Te) quantum dot predecessor islands. Typical "black-white" contrasts (marker BW and arrow) and "coffee-bean" contrasts (marker CB and arrows) indicate that the islands are strained and differ in size.

Fig. 5a shows a small region of the wetting layer between islands in high resolution in the [111] zone axis orientation. The three approximately 0.22 nm wide ± {-220} lattice spacings that are together with the 2D point group p6m revealing of a high-resolution TEM image of the [111] zone axis of a crystal with halite structure are clearly resolved in both the image and its inset Fourier transform power spectrum. This image was recorded at the goniometer setting $\alpha = 6.1°$ (eucentric axis), $\beta = -2.8°$ axis (perpendicular to α-axis) of the double-tilt TEM holder. Tilting the crystal anticlockwise around the (-220) net-plane normal by an amount of 19.5° from this goniometer setting resulted in the [112] zone axis being visible at the goniometer setting $\alpha = 4.7°$, $\beta = 16.5°$. Fig. 5b shows some of the smaller strained islands (i.e. those islands that revealed "black-white" contrasts under two-beam diffraction contrast conditions) in high resolution. The approximately 0.22 nm wide ± (-220) lattice spacing and the 0.36 nm wide ± (11-1) lattice spacing that are together with the 2D point group pm revealing of a high-resolution TEM image of the [112] zone axis of a crystal with halite structure are clearly resolved in both the image and its inset Fourier transform power spectrum. Image-based nanocrystallography by means of transmission electron goniometry [21,22] thus proved that the wetting layer and the strained island both possess the halite structure.

Adjacent to the areas with ordinarily strained islands, there were specimen regions that showed under diffraction contrast imaging condition no typical strain field contrasts, Fig. 6a. Since there are no visible strain fields, our hypothesis is that these entities are some kind of (atomically ordered) Pb-Se-Te compound precipitates with lattice constants and respective orientation relationships that are elastic mismatch strain energy minimizing with respect to the surrounding halite structure Pb(Se,Te) matrix. It is not clear if these entities are embedded in the wetting layer, which would require that they are quasi-two dimensional, or if they are sitting on top of the wetting layer. These entities may, however, be considered as predecessors of atomically ordered quantum dots in this materials system. Consistent with our hypothesis on atomic ordering, the selected area electron diffraction pattern of the same area showed a variety of superlattice reflections, Fig. 6b, that cannot arise from a crystal with the halite structure. Superlattice reflections were also observed in Fourier transform power spectra of [111] zone-axis high-resolution phase-contrast images from the same specimen region. [112] zone-axis selected area electron diffraction pattern from the same specimen region also showed superlattice spots and streaks perpendicular to the transmitted electron beam direction.

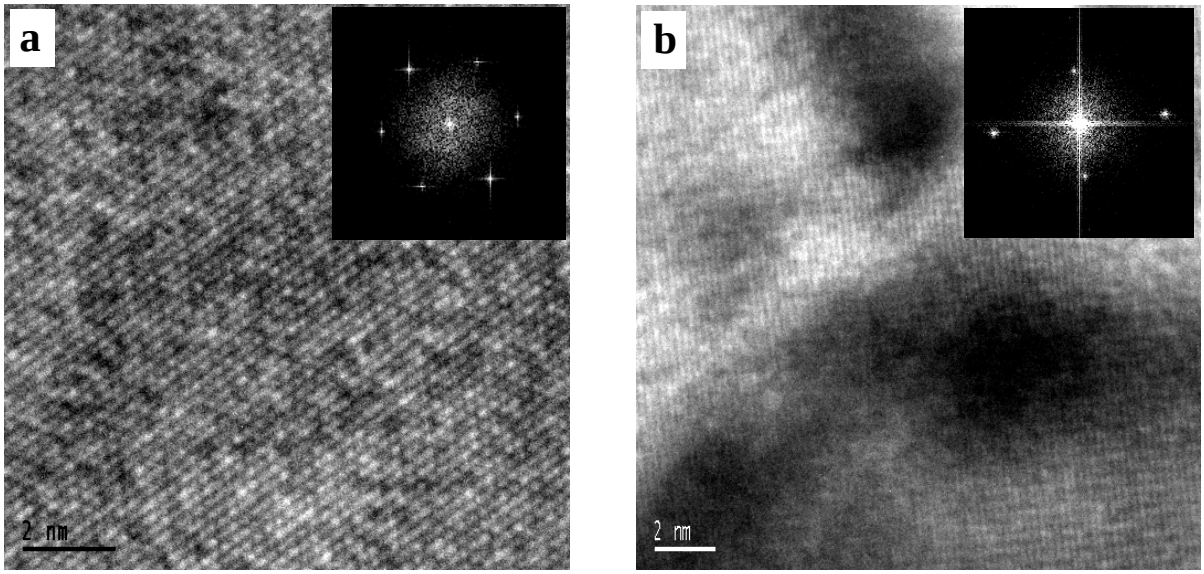

Figure 5. **(a)** [111] zone axis, high-resolution phase-contrast image with inset Fourier transform power spectrum (double-tilt holder goniometer setting: $\alpha = 6.1°$, $\beta = -2.8°$). **(b)** [112] zone axis, high-resolution phase-contrast image with inset Fourier transform power spectrum (double-tilt holder goniometer setting: $\alpha = 4.7°$, $\beta = 16.5°$). From the symmetry of these zone-axis images at these goniometer settings alone, one can conclude that the sample must possess a cubic structure. From the lattice fringe spacings, one can conclude that both the wetting layer and the strained islands possess the halite (rock salt) structure. "Pseudo black-white" contrast is visible in **(b)**, indicating the presence of small strained Pb(Se,Te) quantum dot predecessor islands.

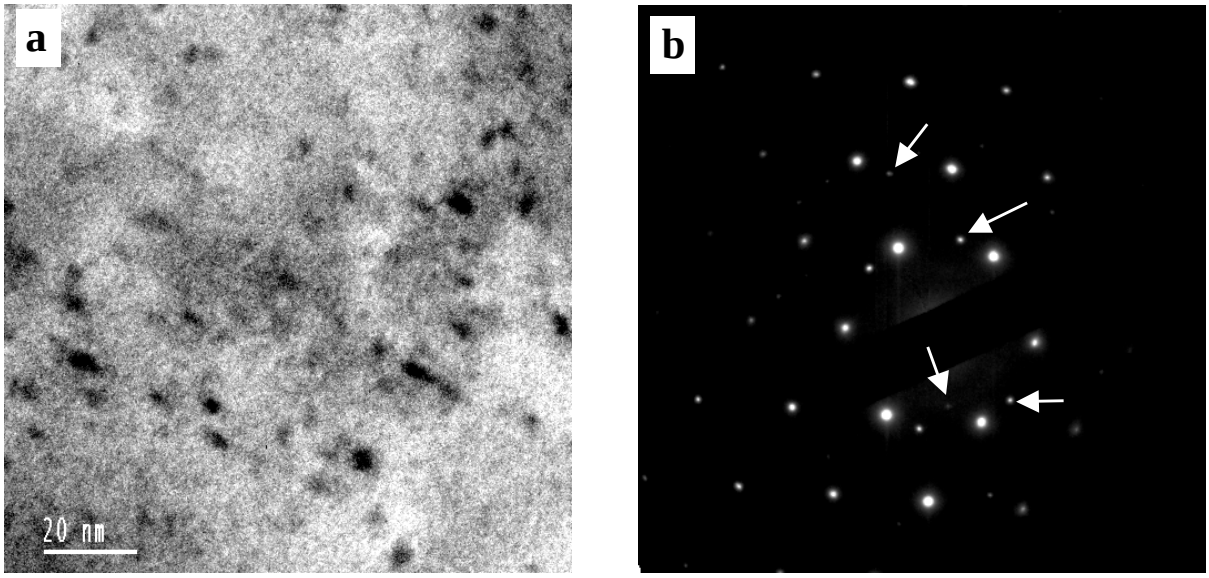

Figure 6. **(a)** Near [111] {220} bright-field diffraction contrast image of Pb(Se,Te). There are no "black-white" and "coffee-bean" contrasts which would identify strain fields. The visibility of approximately 5 nm wide entities suggests differences in the chemical composition. **(b)** [111] zone-axis selected area electron diffraction pattern showing a variety of superlattice reflections that we assume to be due to (atomically ordered) Pb-Se-Te compounds. A few of these superlattice spots (which are forbidden in the halite structure) are marked by arrows. (The faint vertical lines in this diffraction pattern are artifacts of the charge-coupled-device camera used for the recording of this image.)

SUMMARY AND CONCLUSIONS

A Pb(Se,Te) quantum dot predecessor structure was grown by MBE. The coexistence of smaller and larger ordinarily strained Pb(Se,Te) islands with apexes, i.e. ordinarily strained quantum dot predecessor structures, was observed by both AFM and TEM. The dominant variety of islands possesses an average height of 16.9 nm with a standard deviation of 4.6 nm and a relative spread of 27.2 %. The number density of these islands is 126.9

μm^{-2} (or roughly 10^{10} cm^{-2}). Image-based nanocrystallography by means of transmission electron goniometry proved that the 2D wetting layer and the strained 3D nano-islands both possess the halite (rock salt) structure. Regions with small entities that consist probably of (atomically ordered) Pb-Se-Te compounds were also identified in the same specimen. These entities may be considered as constituting predecessors of atomically ordered quantum dots. Optimization of the MBE growth procedure shall result in island distributions as uniform as reported by other authors. A piece of wafer with epitaxially grown {100} faceted nanometer sized islands on a (111) oriented substrate on which, in addition, certain crystallographic directions are marked by partial cleavage or some other means can serve as a nanometrology standard for scanning probe microscopy.

ACKNOWLEDGMENTS

This research was supported by an award from Research Corporation. The TEM investigations were supported by a Campus Research Board of UIC grant (to PM) and NSF Grant DMR-9733895 (to NDB). The MBE growth was supported by NSF grants DMR-9802396 and DMR-0080054 (to PJM).

REFERENCES

1. V.A. Shchukin, N.N. Ledentsov, and D. Bimberg, *Epitaxy of Nanostructures*, Springer, 2003.
2. J. Stangl, V. Holý, and G. Bauer, Structural properties of self-organized semiconductor nanostructures, *Reviews of Modern Physics* **76**, 725 (2004).
3. M.S. Skolnick and D.J. Mowbray, Self-assembled Semiconductor Quantum Dots: Fundamental Physics and Device Applications, *Annu. Rev. Mater. Res.* **34**, 181 (2004).
4. V.M. Ustinov, A.E. Zukov, A.Yu. Egorov, and N.A. Maleen, *Quantum Dot Lasers*, Oxford University Press, Oxford, 2003.
5. M. Grundmann, ed. *Nano-Optoelectronics: Concepts, Physics, and Devices*, Springer, Berlin, 2002.
6. M. Pinczolits, G. Springholz, and G. Bauer, Molecular beam epitaxy of highly faceted self-assembled IV –VI quantum dots with bimodal size distribution, *J. Cryst. Growth* **201-202**, 1126 (1999).
7. M. Pinczolits, G. Springholz, and G. Bauer, Direct formation of self-assembled quantum dots under tensile strain by heteroepitaxy of PbSe on PbTe (111), *Appl. Phys. Lett.* **73**, 250 (1998).
8. K. Alchalabi, D. Zimin, G. Kostorz, and H. Zogg, Self-assembled semiconductor quantum dots with nearly uniform sizes, *Phys. Rev. Lett.* **90**, 26104 (2003).
9. K. Alchalabi, D. Zimin, and H. Zogg, Self Assembled PbSe Quantum Dots with almost Equal Sizes Grown by MBE on PbTe/Si (111), *Mater. Res. Soc. Proc.* **737**, E5.5.1 (2003).
10. G. Springholz, T. Schwarzl, W. Heiss, G. Bauer, M. Aigle, H. Pascher, and I. Vavra, Midinfrared surface-emitting PbSe/PbEuTe quantum-dot lasers, *Appl. Phys. Lett.* **79**, 1225 (2001).
11. P. Möck, T. Topuria, N. D. Browning, M. Dobrowolska, S. Lee, J. K. Furdyna, G. R. Booker, N. J. Mason, and R. J. Nicholas, Internal self-ordering in In(Sb,As), (In,Ga)Sb, and (Cd,Zn,Mn)Se nano-agglomerates/quantum dots, *Appl. Phys. Lett.* **79**, 946 (2001).
12. P. Moeck, Quantum Dots, Semiconductor: Atomic Ordering Over Time, in: *Encyclopedia of Nanoscience and Nanotechnology*, Marcel Dekker, 2004.
13. P. Moeck, Structural and Morphological Transformations in Endotaxial Element and Epitaxial III-V Compound Semiconductor Quantum Dots, Special Issue on Nanotechnology, Nanoscience and Nanobiology of *Problems of Nonlinear Analysis in Engineering Systems*, guest editor S. Santoli, *in press.*
14. A. Zunger and S. Mahajan, Atomic ordering and phase separation in epitaxial III-V alloys, in *Handbook on Semiconductors*, Elsevier, 1994.
15. A. Mascarenhas (editor), *Spontaneous Ordering in Semiconductor Alloys*, Kluwer, 2002.
16. L. Salamanca-Young, D.L. Partin, and J. Heremans, Ordering and stability of $Pb_{1-x}Eu_xTe$, *J. Appl. Phys.* **63**, 1504 (1988).
17. A. Krost, B. Harbecke, R. Faymonville, H. Schlegel, E.J. Fantner, K.E. Ambrosch, and G. Bauer, Growth and Characterization of $Pb_{1-x}Eu_xTe$, *J. Phys. C* **18**, 2119 (1985).
18. A.G. Cullis, D.J. Norris, T. Walter, M.A. Migliorato, and M. Hopkinson, Epitaxial island growth and the Stranski-Krastanow Transition, *Phys. Rev.* **B 66**, 081305-1 (2002).
19. J.G. Griffith and D.A. Grigg, Dimensional metrology with scanning probe microscopes, *J. Appl. Phys.* **74**, R83 (1993).
20. P. Moeck, US patent application, filed November 22, 2004, on behalf of PSU by Klarquist Sparkman, LLP, 121 SW Salmon Street, Suite 1600, Portland, OR 97204, PSU/KS internal ref. OHSU # 852.
21. P. Moeck, W. Qin, and P. Fraundorf, Image-based nanocrystallography in future aberration-corrected transmission electron microscopes, *Mat. Res. Symp. Proc. Vol.* **818**, M11.3.1 (2004).
22. P. Moeck, W. Qin, and P. Fraundorf, Towards 3D image-based nanocrystallography by means of transmission electron goniometry, *Mat. Res. Symp. Proc. Vol.* **829**, B9.4.1 (2005).